International Journal of Heat and Mass Transfer 52 (2009) 200–209

Contents lists available at ScienceDirect

International Journal of Heat and Mass Transfer

journal homepage: www.elsevier.com/locate/ijhmt

Prediction of wall shear for horizontal annular air–water flow

D. Schubring, T.A. Shedd *

Multiphase Flow Visualization and Analysis Laboratory, University of Wisconsin–Madison, 1500 Engineering Drive, Madison, WI 53706-1609, USA

ARTICLE INFO

Article history:
Received 15 January 2008
Received in revised form 21 May 2008
Available online 26 August 2008

Keywords:
Air–water
Shear modeling
Horizontal flow
Annular flow
Correlations

ABSTRACT

In this study, non-intrusive pressure drop, liquid base film thickness distribution, and wave behavior measurements have been obtained for 206 horizontal annular two-phase (air–water) flow conditions in 8.8, 15.1, and 26.3 mm ID tubes. Wall shear was correlated to within 8% by a friction factor involving flow quality and gas Reynolds number. This correlation was found to perform better than those available in the literature, including film roughness correlations, two-phase multiplier methods, and pure data fits. Among published relations, the Müller-Steinhagen and Heck correlation was found to be the most accurate, while the Lockhart–Martinelli correlation can be modified to provide reasonable results. The gas friction velocity is found to be similar to the disturbance wave velocity, which suggests that waves are important sources of shear.

1. Introduction

In the study of two-phase flow phenomena, wall shear (or pressure gradient) is one of the foremost quantities of interest. There has been diverse interest in both horizontal and vertical annular flow, owing to the number of applications in which this regime appears. Numerous studies have been performed, leading to a large array of correlations and models, with both general models and those specific to annular flow. Most of these models can be assigned to one of three categories: two-phase multiplier correlations, film thickness (roughness) correlations, and pure empirical data fits.

Several examples of two-phase multiplier correlations are cited in the paper of Ould Didi et al. [1], who applied these to refrigerants in horizontal tubes. The correlations of Lockhart–Martinelli [2,3] and Grönnerud are examples of simple relations, while the Friedel and Chisholm correlations are more complex. The Chisholm correlation, in particular, involves branched functions depending on the flow conditions.

Correlations involving liquid film roughness first estimate the shear on the gas–liquid interface. Among film thickness correlations, one of the earliest was that of Wallis [4], who proposed a friction factor scaling in an offset linear fashion with film thickness. More complex correlations have evolved, including those of Asali et al. [5] and Hurlburt and Newell [6]. Some have used the proposed interrelationship to derive complete two-fluid models, such as those of Owen and Hewitt [7] and Hurlburt et al. [8].

Empirical data fits often produce the best agreement, but can be limited in their applicability. One example of this type of correlation is that of Müller-Steinhagen and Heck [9].

A total of 206 horizontal air–water flows in three different diameter tubes were studied. In order to ensure that only fully annular data are considered, only those flows with gas kinetic energies above 600 J m^{-3} are used. For each flow condition, pressure gradient, film thickness distribution, and interfacial wave data were obtained. The pressure drop data are compared with examples from each of the three model types and a new empirical correlation is developed specific to this databank.

Other comparisons of shear or frictional pressure gradient correlations exist in the literature. One of the earliest was that of Dukler et al. [10], who compared 9000 flow conditions to a variety of early correlations. Fu and Klausner [11] compared several correlations to develop a vertical flow model, selecting a modified version of a correlation by Henstock and Hanratty [12] as the best fit for their data. Ould Didi et al. [1] applied a number of correlations to horizontal two-phase refrigerant flow.

One of the most extensive correlation comparisons was performed by Ferguson and Spedding [13]. Data from two horizontal test sections with diameters of 45.5 and 93.5 mm were considered. Many correlations were tested for conditions in 16 flow regimes, differentiated by visual observation, leading to regime-dependent recommendations. For annular flow, the model of Olujic [14] is recommended. This model includes two branches, based on a complex criterion for comparison of the velocities of the two phases. For annular flow, the velocities of the two phases are quite different, so Olujic's α-region flow model, a two-phase multiplier method, is used.

Comparisons of frictional pressure drop correlations for other two-phase conditions have also been performed. Qu and Mudawar

* Corresponding author.
E-mail address: shedd@engr.wisc.edu (T.A. Shedd).

0017-9310/$ - see front matter © 2008 Published by Elsevier Ltd.
doi:10.1016/j.ijheatmasstransfer.2008.05.040

Nomenclature

A	flow area (m^2)
D	tube diameter (m)
dP/dz	axial pressure gradient (Pa m^{-1})
G	mass flux ([kg m^{-2} s^{-1}])
KE_{sg}	gas kinetic energy density (J m^{-3})
$\dot{m}$	mass flow rat (kg s^{-1})
P	pressure (Pa)
Re_G	Reynolds number based on total mass flux ()
U_s	superficial velocity (m s^{-1})
v_{fric}	gas friction velocity (m s^{-1})
v_w	wave velocity (m s^{-1})
x	flow quality ()

Greek symbols

δ	film thickness (m)
μ	dynamic viscosity (kg m^{-1} s^{-1})
ρ	density (kg m^{-3})
τ_i	interfacial shear (Pa)
τ_w	wall shear (Pa)

Subscripts

corr	pertains to a correlation ()
exp	pertains to experimental result ()
frict	pertains to frictional part ()
g	pertains to gas phase ()
l	pertains to liquid phase ()

[15] compared correlations for micro-channels and developed their own specialized correlation. Chen et al. [16] performed experiments in normal and microgravity conditions, comparing both sets of data to correlations from the literature.

In the present work, wall shear was selected for comparison. These data are estimated based on pressure loss measurements, rather than by direct measurements of shear (as in the work of Vlachos et al. [17], Govan et al. [18], and others). Correlations in the literature are most often presented as estimates of pressure loss (two-phase multipliers, pure empirical fits) or interfacial shear (film roughness relations); wall shear can be linked to both of these through force balances (see Section 3.1). Further, wall shear can be expected to be the relevant quantity for detailed liquid film modeling (velocity profiles, etc.).

This study is differentiated from those in the literature due to the availability of wave data (frequency and velocity) and base film thickness distributions for all flow conditions considered. Only fully annular flow is explored, which contrasts with comparisons in the literature that attempt to select one correlation for multiple flow regimes. By comparing these shear data to correlations that assume different physical mechanisms (e.g., film thickness), the dependence of shear on these other parameters can be explored. Observations stemming from shear-related quantities (e.g., gas friction velocity) can further recommend paths for data acquisition and analysis (e.g., disturbance wave velocity).

2. Experimental setup

2.1. Flow loop

The two-phase flow loop used for these experiments is shown in Fig. 1. Laboratory compressed air was delivered to the test section inlet via a bank of variable-area volumetric flow meters. The uncertainties, based on manufacturer's stated values and including density correction, were 8.4 L min^{-1} below 250 L min^{-1} flow, 14 L min^{-1} between 300 and 700 L min^{-1} flow, and 68 L min^{-1} above 700 L min^{-1} flow. A pressure gauge near the flow meters allowed for the correction of flow meter readings to compensate for variations in air density and for the calculation of the mass flow rate entering the test section. Water entered the flow loop through a series of small (1.5 or 3 mm) holes drilled in the test section wall about 150 mm from the air entrance.

The two-phase air/water mixture passed through a flow development length before any measurements were obtained. This length was 400 diameters for the 8.8 mm I.D. tube, 330 diameters for the 15.1 mm I.D. tube, and 210 diameters for the 26.3 mm I.D. tube. The air and water were separated in a gravity-assisted centrifugal separator, after which the water entered a holding reservoir. A variable-speed peristaltic pump was used to draw water from the reservoir through a 40-μm filter. Because of the pulsating nature of peristaltic pumps, a pulse dampening closed reservoir was placed after the pump. The liquid flow was measured using a bank of variable-area rotameters with manufacturer's specified accuracies of 45 cm^3 min^{-1} for less than 1500 cm^3 min^{-1} flow, 90 cm^3 min^{-1} for 1500 to 3000 cm^3 min^{-1} flow, and 5% of reading for above 3000 cm^3 min^{-1} flow. The test sections were constructed of clear PVC (Excelon R4000) for complete visualization of the flow from liquid entrance to exit.

The issues of development length and method of liquid introduction were studied by Okada and Fujita [19]. Their experiments considered gas superficial velocities similar to the present work, although with a slightly larger tube and lower liquid flow rates. They determined that the method of liquid injection was of little consequence to fully developed friction factors, recommending a development length of 300 diameters. However, examination of Fig. 8 of [19] indicates that for the higher liquid velocities, similar to those in the present study, a development length to 200 diameters is likely sufficient.

2.2. Pressure measurement

A bourdon-tube gauge was placed near the test section so that a good estimate of local air density could be obtained. In the 15.1- and 26.3-mm I.D. tubes, this gauge was placed at the beginning of the test section, while it was placed 0.5 m upstream for the 8.8 mm I.D. tube. The 8.8 mm I.D. case is shown in Fig. 1. Using the two static pressure measurements, dry air mass was conserved in the calculations. The air entering the test section was assumed to be dry at a temperature of 20 °C. Within the test section, a relative humidity of 100% was assumed at a temperature of 11 °C, based on average liquid temperature measurements.

2.3. Data range

For each diameter, an array of meter readings were selected to provide a large bank of data. The 206 fully annular data points are a subset of this data. Fig. 4 shows wall shear against two common correlating parameters: gas kinetic energy and film thickness. Superficial gas and liquid velocities were calculated according to Eqs. (1) and (2), with gas kinetic energy calculated according to Eq. (3). Flow quality and total mass flux are defined by Eqs. (4) and (5), respectively.

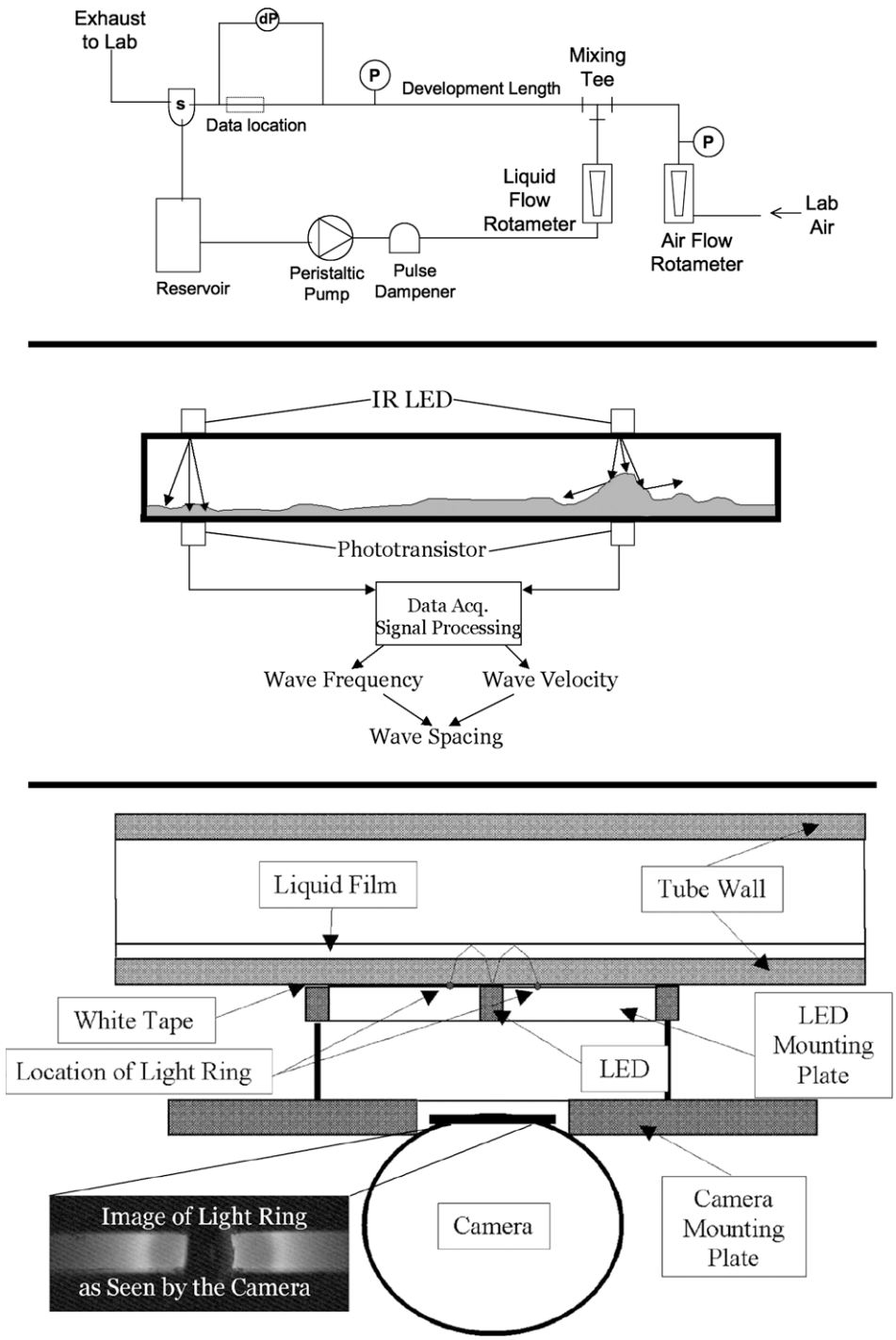

Fig. 1. (Top) Diagram of flow loop. (Middle) Wave data acquisition system. (Bottom) Base film thickness data acquisition system.

$$U_{sg} = \frac{Gx}{\rho_g} \quad (1)$$

$$U_{sl} = \frac{G(1-x)}{\rho_l} \quad (2)$$

$$KE_{sg} = \frac{U_{sg}^2 \rho_g}{2} \quad (3)$$

$$x = \frac{\dot{m}_g}{\dot{m}_g + \dot{m}_l} \quad (4)$$

$$G = \frac{\dot{m}_g + \dot{m}_l}{A} \quad (5)$$

In many experimental studies, particularly for pure fluids, it is conventional to generate arrays of total mass flux and flow quality rather than meter readings. Tables 2 (8.8 mm I.D.), 3 (15.1 mm I.D.), and 4 (26.3 mm I.D.) show the values of total mass flux, flow quality, and test section pressure for all fully annular flows considered.

Superficial gas velocities of between 28 and 86 m s^{-1} were considered, with superficial liquid velocities between 0.03 and 0.30 m s^{-1}. Superficial gas kinetic energy densities ranged from 600 to 5400 J m^{-3} as a result of the variable superficial velocities and gas densities through the test section. The cut-off of 600 J m^{-3} was selected to correspond with a change in trends of

Table 1
Mean, mean absolute, and RMS errors for correlations

Correlation	Mean (%)	MAE (%)	RMS (%)
Grönnerud	−42.58	42.58	44.86
Olujic	0.00	20.90	25.22
Lockhart–Martinelli	−34.66	34.66	36.62
Chisholm	23.41	25.67	36.98
Wallis	135.91	136.20	178.68
Hurlburt and Newell (1)	−8.71	16.67	19.67
Hurlburt and Newell (2)	−20.11	24.44	28.40
Hurlburt et al.	−21.62	29.58	33.51
Müller-Steinhagen and Heck	6.98	10.75	15.46
Schubring and Shedd	0.03	7.68	10.26

Table 2
Mass flux (kg m^{-2} s^{-1}), flow quality, and test section pressure (kPa) for 8.8 mm I.D. tube

	1100	900	700	600	500	400	320	240	160
250	430, 0.299, 133.6	375, 0.343, 134.8	319, 0.400, 128.3	285, 0.424, 124.5	256, 0.464, 118.1,	224, 0.510 119.5	198, 0.558, 114.7	173, 0.620, 113.7	147, 0.702, 111.1
230	416, 0.275, 130.8	361, 0.316, 127.8	306, 0.373, 124.7	270, 0.392, 118.6	239, 0.426, 113.8	209, 0.475, 112.7	184, 0.523, 111.6	159, 0.587, 110.1	135, 0.674, 109.1
200	401, 0.248, 126.2	344, 0.284, 124.6	286, 0.328, 120.3	254, 0.353, 117.5	225, 0.390, 115.8	193, 0.431, 112.6	169, 0.480, 111.0	144, 0.544, 109.1	119, 0.633, 107.7
180	383, 0.213, 120.5	328, 0.248, 119.6	273, 0.297, 114.7	240, 0.316, 114.1	211, 0.349, 110.8	181, 0.393, 108.5	157, 0.443, 107.2	134, 0.508, 105.2	110, 0.602, 105.4
150	369, 0.184, 117.6	313, 0.211, 116.1	256, 0.250, 113.3	226, 0.272, 112.1	197, 0.304, 110.2	168, 0.347, 110.0	145, 0.394 107.7	121, 0.458, 107.0	98, 0.552, 105.0
130	356, 0.153, 113.8	300, 0.177, 112.4	245, 0.217, 111.2	215, 0.237, 109.0	186, 0.265, 106.5	158, 0.305, 105.8	135, 0.350, 105.2	112, 0.414, 104.5	89, 0.509, 104.1
100	342, 0.119, 111.6,								

Liquid meter readings (cm^3 min^{-1}) along top, air meter readings (L min^{-1}) along side.

pressure drop, film thickness distribution, and wave behavior that may be indicative of a transition from fully annular behavior and a separate wavy-annular regime.

2.4. Pressure drop measurement

The differential pressure measurement was performed over 1 m for the 15.1 and 26.3 mm I.D. tubes and over 0.5 m for the 8.8 mm I.D. tube, spanning the area of the tube used as the test section for film thickness and wave measurements. Two strain-gauge-based differential pressure sensors were connected in parallel so that the pressure gradient could be determined with low uncertainty across a wide range of flows. The pressure measurements were averaged over at least fifteen seconds to account for fluctuations due to waves. Propagating both instrument and statistical uncertainties, the total uncertainty of the pressure difference measurement is of order 2%.

2.5. Film thickness measurement

Using a technique outlined by Shedd and Newell [20], base film thickness measurements were made at the top, bottom, and side of the tube for each flow condition. This non-intrusive method uses the pattern of diffuse light reflected from the liquid surface to determine the liquid film thickness (Fig. 1). These data were used with film roughness correlations from the literature.

Rodríguez and Shedd [21] have shown, by comparisons with measurements using planar fluorescence imaging, that this optical method accurately determines the mean film thickness between large liquid waves. This contrasts with the average film thickness (base film and waves) commonly used in these correlations. While this can be expected to reduce the accuracy of the relations used, it allows for a separation of the effects of waves and base film on average shear stress.

Uncertainties vary with the film thickness and surface roughness (waviness). Typical base film thickness uncertainties are around 2% for high gas flows and 5% for low gas flows, both within the fully annular regime. The mean relative difference between average film thickness and maximum (bottom) film thickness was 18% with a maximum of 82%.

2.6. Wave measurements

An optical method, similar to that reported by Hawkes et al. [22], was used to study wave frequency, velocity, and spacing. Two LED/phototransistor pairs were mounted on the outside of the tube, 0.115 m apart (Fig. 1). Light from an LED passes through the transparent tube wall, through the air/water mixture, and on to the phototransistor. When the surface of the liquid is not smooth, some of the light is refracted or reflected away from the phototransistor, causing a change in its output current. Using digital video imaging simultaneously with the LED/phototransistor measurement, it was confirmed that the phototransistor signal was very well correlated with liquid waves. Two wave sensors were used so that wave velocity and spacing could be obtained from the optical signals. A mean wave frequency, f, was derived by analyzing the signal from each sensor individually using the Fast Fourier Transform (FFT) algorithm to generate a mean power spectral density for a large number of trials. By cross-correlating the signals, a wave velocity, v_w, was derived. Between 100 and 250 trials were run for each annular test condition, each lasting between 1 and 2 s.

Occasionally, the cross-correlation of waveforms would pair incorrect waves in the two sensors, calculating an inaccurate velocity. The FFT algorithm would also occasionally calculate an incorrect frequency, usually a harmonic of the true frequency. In order to prevent a small number of data points from skewing the average, the largest and smallest 2–3% data was removed, generating a clipped mean. Within the annular regime, this clipped mean was very close to the median value.

3. Calculations

3.1. Experimental shear

From the experimental pressure drop, average base film thickness (δ), and flow data, experimental interfacial shear was calculated by

$$\tau_{i,exp} = -\frac{D-2\delta}{4}\left(1-\frac{\rho_g U_{sg}^2}{P}\right)\frac{dP}{dz_{exp}} \tag{6}$$

Note that this equation assumes ideal gas behavior in the air and accounts for acceleration pressure losses of the gas. Since the maximum superficial air velocity does not exceed 25% of air's sonic velocity at the temperature of interest, a more rigorous treatment of compressibility effects is not needed.

Experimental wall shear was calculated by

$$\tau_{w,exp} = \tau_{i,exp}\frac{D-2\delta}{D} - \frac{1}{4}\frac{dP}{dz_{exp}}\frac{D^2-(D-2\delta)^2}{D} \tag{7}$$

Table 3
Mass flux (kg m^{-2} s^{-1}), flow quality, and test section pressure (kPa) for 15.1 mm I.D. tube

	2900	2500	2100	1800	1500	1200	900	700	500	350
700	387, 0.302, 130.7	348, 0.331, 127.2	308, 0.365, 125.5	279, 0.399, 123.8	250, 0.441, 122.0	220, 0.493, 120.3	190, 0.559, 118.6	169, 0.615, 115.1	148, 0.686, 113.4	132, 0.753, 111.7
650	378, 0.286 128.9	339, 0.313, 125.5	298, 0.345, 122.0	269, 0.378, 120.3	239, 0.417, 118.6	210, 0.467, 116.9	179, 0.533, 115.1	159, 0.591, 113.4	137, 0.661, 111.7	122, 0 733, 110.0
600	367, 0.265, 125.5	328, 0.290, 122.0	288, 0.320, 120.3	259, 0.353, 118.6	229, 0.391, 116.9	200, 0.440, 115.1	169, 0.504, 111.7	149, 0.563, 110.0	128, 0.635, 108.2	112, 0.709, 106.5
560	359, 0.248, 122.0	319, 0.272, 120.3	279, 0.301, 118.6	251, 0.332, 116.9	221, 0.369, 113.4	192, 0.417, 111.7	162, 0.481, 110.0	142, 0.540, 110.0	120, 0.613, 106.5	105, 0.691, 106.5
490	345, 0.217, 118.6	306, 0.239, 116.9	266, 0.266, 115.1	238, 0.296, 113.4	208, 0.330, 111.7	179, 0.376, 110.0	149, 0.438, 108.2	129, 0.496, 108.2	109, 0.571, 104.8	94, 0 653, 101.4
420	332, 0.186, 115.1	294, 0.207, 113.4	254, 0.231, 111.7	226, 0.257, 111.7	197, 0.290, 110.0	167, 0.333, 108.2	138, 0.393, 106.5	119, 0.451, 106.5	98, 0.527, 101.4	84, 0.610, 101.4
360	321, 0.158, 111.7	283, 0.177, 110.0	244, 0.198, 110.0	216, 0.223, 108.2	186, 0.251, 106.5	158, 0.291, 106.5	129, 0.349, 104.8	109, 0.403, 101.4	90, 0.481, 101.4	75, 0 566, 101.4
330	315, 0.144 110.0	277, 0.161, 110.0	237, 0.177, 108.2	210, 0.204, 106.5	182, 0.232, 104.8	153, 0.271, 104.8	124, 0.327, 101.4	105, 0.381, 101.4	86, 0.457, 101.4	71, 0 542, 101.4
300	310, 0.130, 108.2									

Liquid meter readings (cm^3 min^{-1}) along top, air meter readings (L min^{-1}) along side.

Table 4
Mass flux (kg m^{-2} s^{-1}), flow quality, and test section pressure (kPa) for 26.3 mm I.D. tube

	9000	7500	6500	5500	4500	3500	2700	2700	1500	1000
2200	402, 0.313, 122.0	354, 0.349, 118.6	322, 0.380, 118.6	288, 0.414, 115.1	255, 0.460, 115.1	223, 0.519, 113.4	197, 0.580, 113.4	175, 0.649, 111.7	158, 0.708, 111.7	141, 0.782, 110.0
2000	384, 0.281, 116.9	337, 0.317, 115.1	305, 0.347, 115.1	273, 0.382, 113.4	241, 0.427, 111.7	208, 0.484, 111.7	182, 0.544, 110.0	159, 0.614, 108.2	142, 0.676, 108.2	126, 0.756, 106.5
1800	369, 0.252 113.4	321, 0.283, 111.7	289, 0.311, 110.0	258, 0.346, 110.0	226, 0.389, 108.2	194, 0.446, 108.2	168, 0.507, 108.2	146, 0.579, 106.5	129, 0.644, 106.5	113, 0 728, 104.8
1600	355, 0.223, 111.7	308, 0.254, 110.0	277, 0.279, 108.2	245, 0.312, 108.2	214, 0.354, 108.2	182, 0.410, 106.5	156, 0.469, 106.5	133, 0.540, 104.8	117, 0.607, 101.4	101, 0.698, 101.4
1400	342, 0.193, 108.2	296, 0.222, 106.5	264, 0.245, 106.5	233, 0.275, 106.5	201, 0.315, 104.8	170, 0.370, 104.8	145, 0.428, 104.8	123, 0.499, 101.4	106, 0.568, 101.4	91, 0 662, 101.4
1200	331, 0.165, 106.5	284, 0.190, 104.8	253, 0.212, 104.8	222, 0.240, 104.8	191, 0.278, 101.4	160, 0.328, 101.4	134, 0.383, 101.4	112, 0.453, 101.4	96, 0.523, 101.4	81, 0.620, 101.4
1000	320, 0.137, 101.4	273, 0.159, 101.4	243, 0.178, 101.4	212, 0.203, 101.4	181, 0.236, 101.4	149, 0.281, 101.4	124, 0.334, 101.4	103, 0.402, 101.4	87, 0.471, 101.4	71, 0.568, 101.4

Liquid meter readings (cm^3 min^{-1}) along top, air meter readings (L min^{-1}) along side.

For the fully annular data obtained in this study, the difference between wall and interfacial shear is of order 2%. Further, the film thickness is a small fraction of the tube diameter and the average wall shear is of interest. As such, uncertainties introduced because

of the lack of asymmetry information in Eq. (7) can be ignored. In particular, they are small relative to experimental uncertainty from flow rates, etc.

Droplet deposition is neglected in Eq. (6), as reliable data or correlations are not available. A more exact equation including the effects of deposition was developed by Fore et al. [23]. The appropriate term in this equation for interfacial shear is essentially the product of gas velocity and droplet deposition mass flux. The entrainment and deposition correlations suggested by Kataoka et al. [24] can be used for a rough estimate. Based on these, less than 4% of the average shear calculated by Eq. (6) is due to droplet deposition. Therefore, the approximation to neglect deposition is also within the range of experimental uncertainty. In addition, the acceleration of droplets is not accounted for, increasing the uncertainty of the shear results, particularly for higher gas flow rates, for which entrainment is most significant. The authors contend that it is preferable to exclude such second-order effects rather than compounding the number of empirical correlations employed.

3.2. Correlations

The correlations used required calculation of several dimensionless parameters, most commonly Reynolds numbers. The most common Reynolds number used in the correlations is defined in Eq. (8)

$$Re_G = \frac{GD}{\mu_l} \tag{8}$$

The implementations of the Lockhart–Martinelli, Chisholm, and Grönnerud correlations are outlined in the work of Ould Didi [1] and are presented for frictional pressure difference (rather than shear). This form is also seen in the corelations of Olujic [14] and Müller-Steinhagen and Heck [9]. These can be converted to a form for frictional pressure gradient and subsequently converted into a calculation for wall shear.

$$\tau_{w,\,corr} = -\frac{D}{4}\frac{dP}{dz_{frict,corr}} \tag{9}$$

The Wallis [4] correlation, as well as the correlations of Hurlburt and Newell [6], which proceed from the work of Asali et al. [5], use film thickness to calculate interfacial shear. The correlation labeled Hurlburt and Newell (1) uses this dimensionless film thickness as part of a linear term, while that labeled Hurlburt and Newell (2) uses it in an exponential term. For these correlations, correlated interfacial shear was transformed to a wall shear according to Eq. 7, using a self-consistent estimated pressure drop.

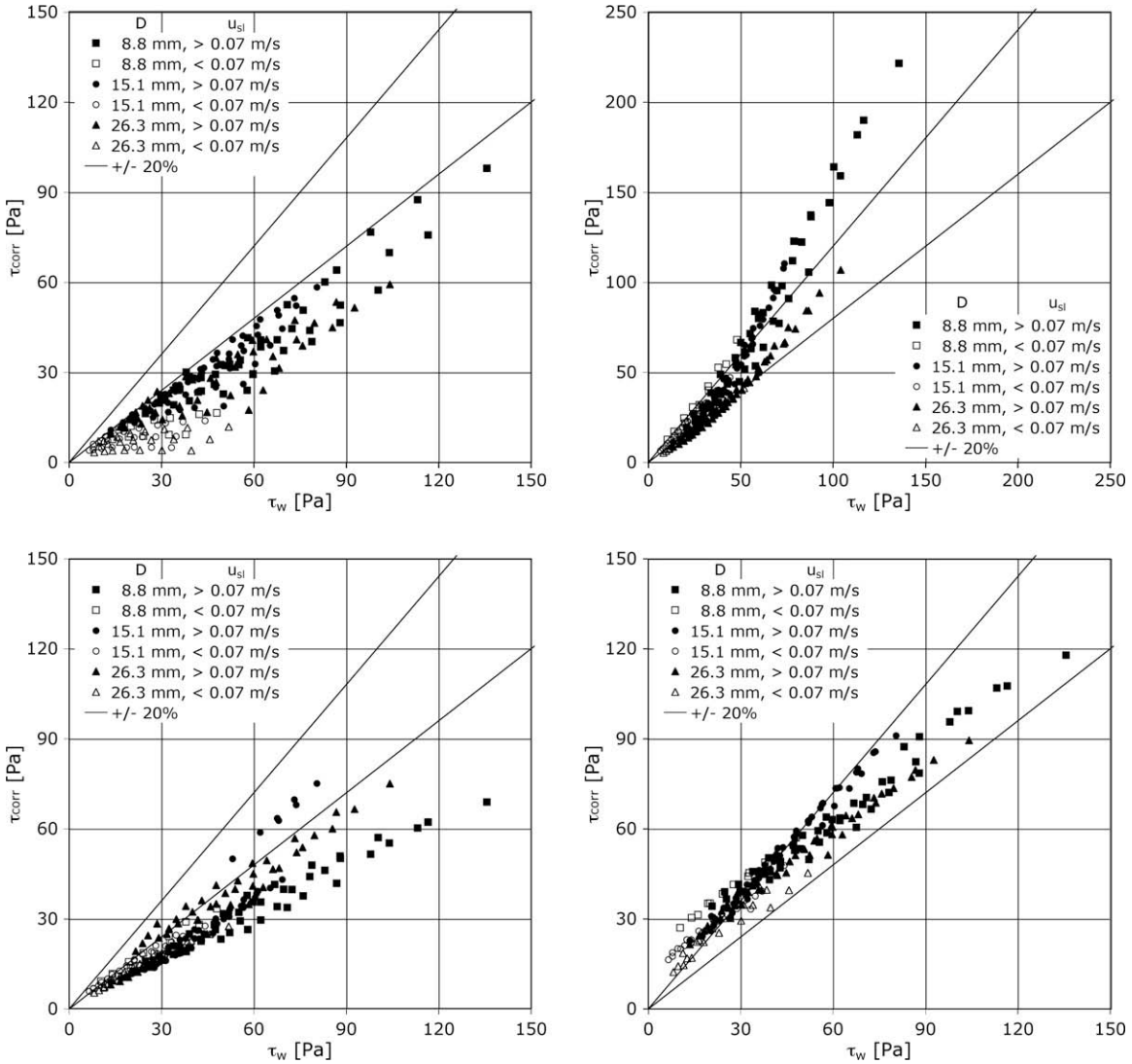

Fig. 2. Performance of two-phase multiplier correlations. (Top left) Grönnerud. (Top right) Olujic. (Bottom left) Lockhart–Martinelli. (Bottom right) Chisholm.

The Hurlburt et al. model [8] (as amended via private communication) was also tested. The model was modified for this work to neglect the effect of droplet deposition, consistent with the other models used, and was adapted to the horizontal case by neglecting gravity. As with the other film roughness correlations, a transformation from interfacial to wall shear was performed.

3.3. Correlation of current data

A correlation of the current data for all three tube sizes was also derived based on dimensional analysis that produced better performance than any of the published correlations (Eq. (10)). The constant was optimized to three significant figures, while the power on Reynolds number was optimized to within ±0.05.

$$\tau_{w,corr} = 0.0217 \frac{KE_{sg}}{x} Re_G^{-0.15} = 0.0109 G U_{sg} Re_G^{-0.15} \quad (10)$$

4. Results and discussion

The performance of the correlations with the current data is shown in Table 1.

4.1. Two-phase multiplier correlations

The correlations for two-phase multipliers are generally simple to implement, as they require only basic property and flow condition information. However, they are not very accurate for the current data set. The Grönnerud correlation, shown in Fig. 2, was not developed for air-water annular flow and does not perform well for these conditions. It consistently underpredicts shear, especially in cases of low liquid flow.

The Lockhart–Martinelli correlation, also shown in Fig. 2, consists of two relationships; the one used depends on liquid Reynolds number. The relation for low liquid Reynolds number underpredicts the shear by between 40% and 60% for its applicable region, while the correlation for higher liquid Reynolds number is accurate to within approximately 20% for its recommended range, but also consistently underpredicts. If the high liquid Reynolds number correlation is used in all cases, the mean error drops to −19.10%, with an MAE of 19.39%.

Among the two-phase multiplier models, the Chisholm and Olujic correlations, also shown in Fig. 2, performed the best, with errors less than 30%. Chisholm tends to underestimate the effect of gas flow on the shear, overestimating shear for low gas flows

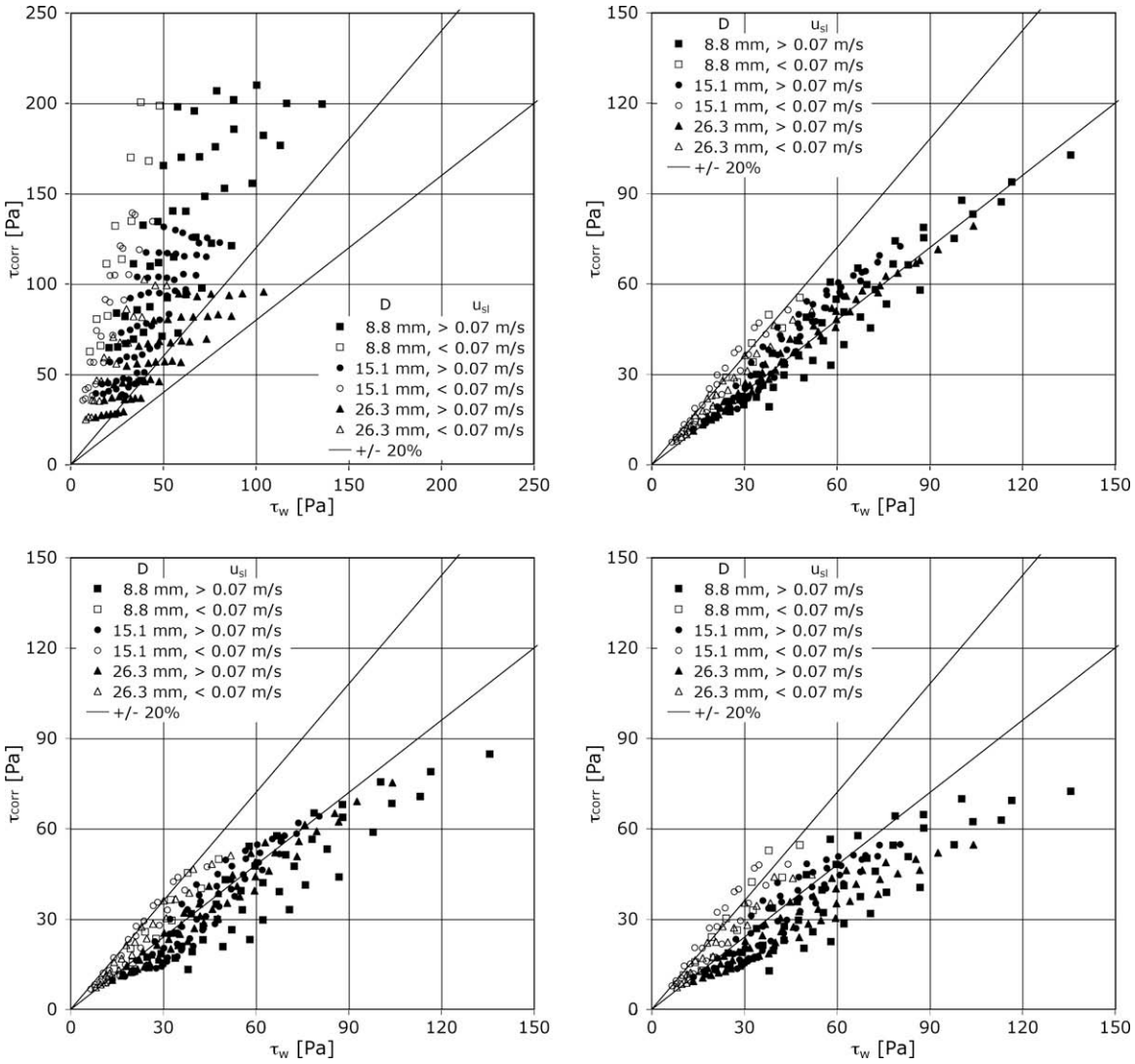

Fig. 3. Performance of film roughness correlations. (Top left) Wallis (note scale). (Top right) Hurlburt and Newell (1). (Bottom left) Hurlburt and Newell (2). (Bottom right) Hurlburt et al.

and underpredicting at high gas flows. It also significantly overpredicts at very low total Reynolds numbers. Olujic does not properly account for the diameter effect nor the effect of liquid flow rate in the present data and also overpredicts for high-shear flows.

4.2. Film roughness correlations

The correlation of Wallis, one of the first attempts at a film roughness approach, performed poorly for the present databank (Fig. 3). The two correlations of Hurlburt and Newell perform acceptably, with errors of order 20%, as seen in Fig. 3. They suffer from similar difficulties, underpredicting for high liquid flows and overpredicting for low liquid flows. The two-zone model of Hurlburt et al. (Fig. 3), originally proposed for vertical flow, has slightly larger errors. By re-optimizing empirical factors in this model, a 20% MAE can be achieved. However, the model is quite complex and does not provide performance comparable to purely empirical relations for the current databank.

A plot of wall shear and base film thickness for the 8.8 mm tube is presented in Fig. 4. For constant air meter reading (approximately constant gas superficial velocity), shear varies across a factor of 3–5. In contrast, base film thickness varies over only 30% for the lowest air flow series and is almost constant for the highest gas flow. Similar data exist for the other two diameters. This suggests that it may not be realistic to model shear as a function of gas flow rate and base film thickness alone.

The film thickness generally used in film roughness correlations is the average film thickness, which includes the thickness of interfacial waves. This measurement is not available from the optical technique used in this study. Film roughness correlations, therefore, group wave and base film behavior together into a single parameter. In so doing, the ability to resolve the separate effects on shear, in any, from each is lost. The relation between shear and wave behavior alone is briefly explored below.

4.3. Friction velocity and waves

Wave velocity data are available for all flow conditions under consideration with liquid superficial velocities above 0.045 m s^{-1}. There is a strong interrelationship between wave behavior and shear (pressure drop) behavior in the form of the gas friction velocity (Eq. (11), Fig. 4) that was first observed by Swanson [25]. Sawai et al. [26] attempted to correlate wave velocity with the liquid friction velocity; for the present databank, this approach is not as successful as the gas friction velocity.

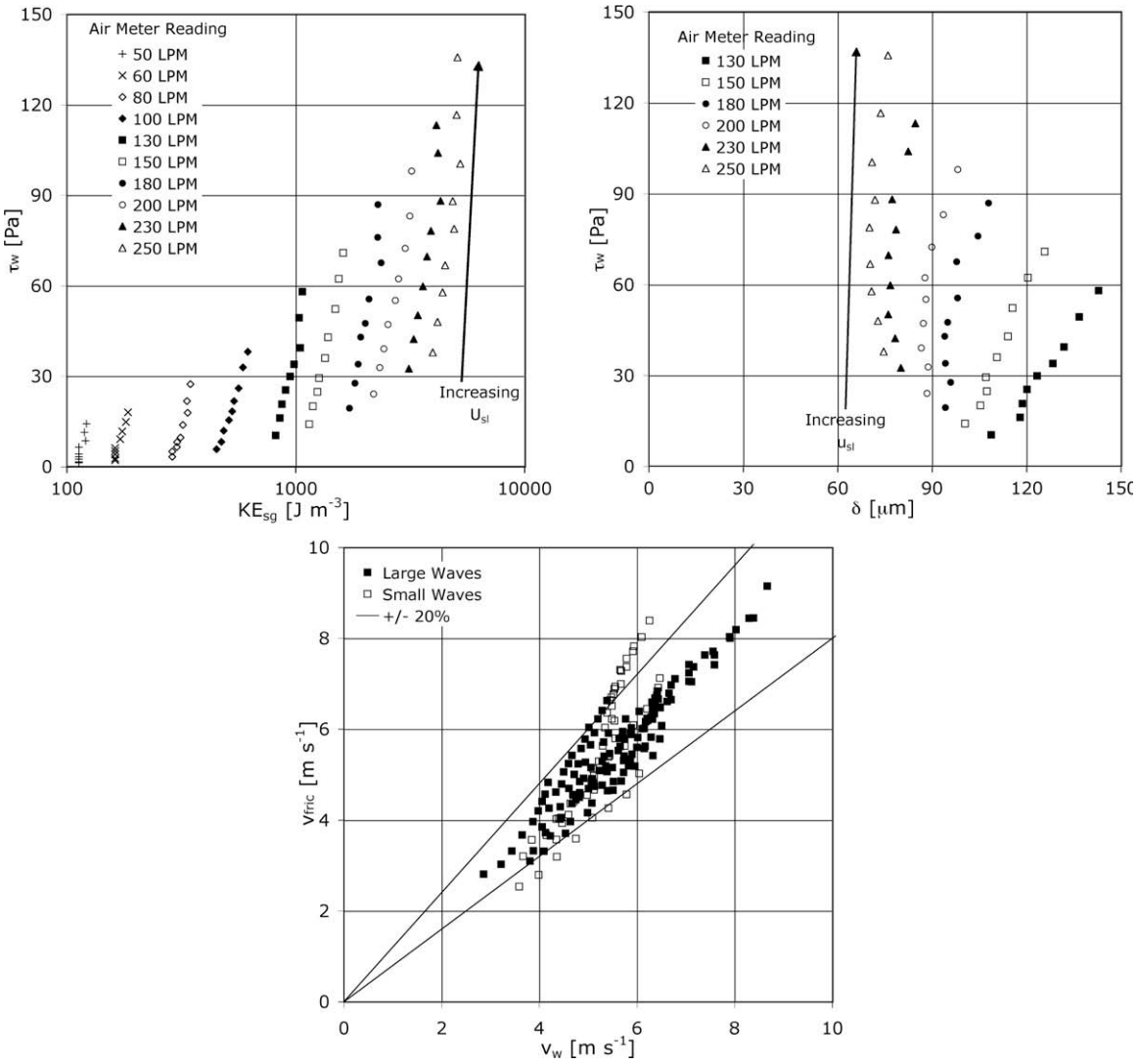

Fig. 4. (Top) Series of constant air meter reading, 8.8 mm tube. (Top left) Shear vs. gas kinetic energy. (Top right) Shear vs. base film thickness. (Bottom) Friction velocity vs. wave velocity.

$$v_{\text{fric}} = \sqrt{\frac{\tau_w}{\rho_g}} \tag{11}$$

For this range of flow conditions, the mean absolute error is 9.02%, with a mean error of less than 1%. It was found that wave measurements were more challenging to obtain for very low liquid Reynolds number or very high gas Reynolds number conditions. For some cases, accurate measurement of frequency was not possible; it is likely that these waves are smaller. Considering only those points for which reliable frequency data are also available (termed Large Waves in Fig. 4), the MAE is 6.54%.

By inverting the friction velocity observation, shear can be correlated with the wave velocity v_w by:

$$\tau_{w,\text{corr}} = \rho_g v_w^2 \tag{12}$$

This correlation performs to within 20% MAE – similar to optimized film roughness correlations when base film thickness is employed. This suggests that the effect of waves on wall shear (pressure loss) is comparable to the effect from base film roughness.

Eq. (12) suggests that wall shear varies as the square of wave velocity; i.e., the kinetic energy density of waves (since their density is constant in the present study). Waves accelerate the base liquid film over which they travel, providing a source of shear. Between waves, the liquid film is no longer exposed to such a strong source of shear; as such, the film will decelerate and the energy will be dissipated. Further research should be undertaken to address these liquid film velocity profiles directly, as well as to explore shear stemming from gas flow over the base film when waves are not present and to address the physics behind the apparent linear dependence on gas density.

A direct link between waves and instantaneous shear measurements was observed by Govan et al. [18]. It was noted that a peak in the power spectral density of the time-varying shear measurements corresponded to an observed wave frequency. A detailed discussion of waves is provided by the review articles of Azzopardi [27,28], which provide references to several databases of wave information (primarily in vertical geometry) and to other correlations and models for wave velocity. In light of the apparent link between wave behavior and shear, the authors believe that direct examination of wave behavior is of value. Detailed characterization of and comparison of other correlations to the present wave data has been presented in a separate work [29].

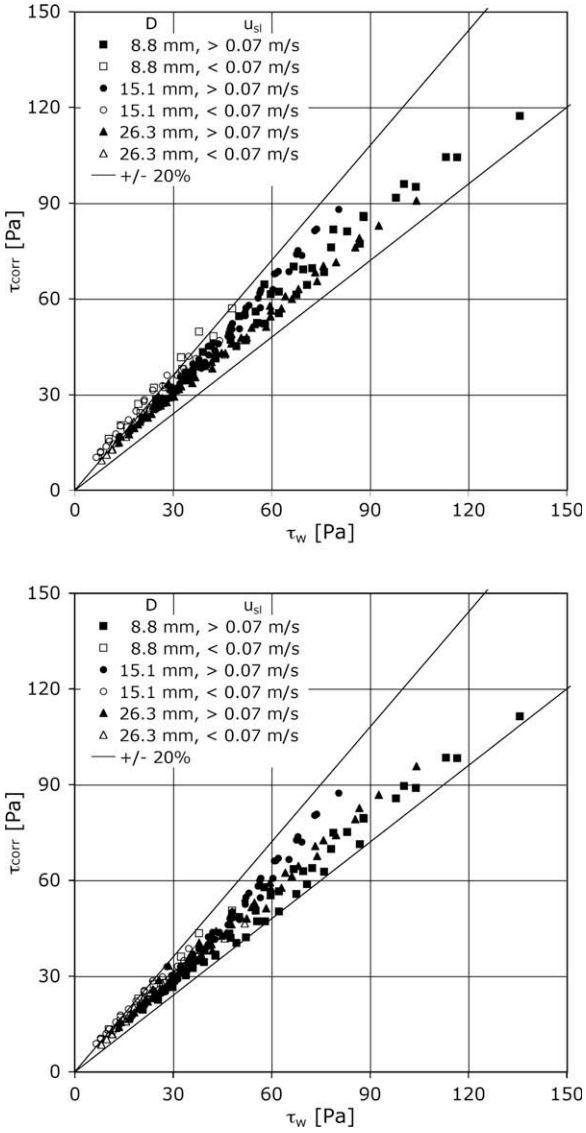

Fig. 5. (Top) Performance of data fit correlations. (Bottom) Müller-Steinhagen and Heck. Current correlation.

4.4. Empirical fit correlations

The Müller-Steinhagen and Heck correlation provides the best results from the literature. It is essentially a curve fit between 0% (single-phase liquid) and 100% (single-phase gas) quality flows. This relation was proposed based on a databank containing over 9000 flow conditions, including both pure fluid and non-condensable gas data. While some of these data were taken for air–water and some are in small diameter tubes, no air–water data were employed from test sections less than 19 mm in diameter.

The current correlation, constructed from dimensional analysis for the present data set only, produces similar overall performance and has a similar region of poor performance. Both can be seen in Fig. 5.

The primary flaw in these correlations is a strong overprediction for cases of low liquid Reynolds number, indicative of small liquid flows in small tubes. It is most apparent for liquid superficial velocities of less than 0.07 m s^{-1}. If these points are ignored in all diameter tubes, the mean absolute error for the present correlation, as well as Müller-Steinhagen and Heck, drops below 7% with no points having an error above 20%.

The two-phase multiplier correlations and empirical data fits have been compared to the data of Laurinat [30]. Of the 67 flows reported in a 25.4 mm inside diameter tube in that work, 27 are found to be within the data range of the present study (i.e., U_{sl} between 0.03 and 0.30 m s^{-1} and KE_{sg} greater than 600 J m^{-3}). The MAE of the present correlation with respect to Laurinat's data is less than 15%, comparable to that of the Müller-Steinhagen and Heck correlation and superior to that of the two-phase multiplier methods considered. Further, Laurinat's data extend to a KE_{sg} of nearly 18,000 J m^{-3}; the present relation correlates these higher gas flow data well.

Comparing Eq. (10) to a single phase gas calculation, the KE_{sg} term is changed to a GU_{sg} term, with modifications to the constant and Reynolds number factors. The G factor is analogous to the volumetric momentum density ρu from single-phase flow. Single-phase calculations also require a velocity, and since most of the mass travels at a velocity proportional to U_{sg} (gas, waves, entrained droplets) and the gas velocity is more than an order of magnitude higher than the characteristic film velocity, the inflow and outflow of momentum is likely to be controlled by a gas velocity.

5. Summary

- The correlation of Lockhart and Martinelli performs poorly as presented, but the high-liquid branch of this correlation can be adapted to provide reasonable results.
- The correlations based on film thickness tend to underestimate the dependence of shear on liquid flow rate when base film thickness measurements are used.
- Wave velocity is well correlated by the gas friction velocity within the annular regime, which may indicate a direct link between wave and wall shear behavior.
- The best previously published correlation for comparison to the current data set is that of Müller-Steinhagen and Heck.
- The best correlation for shear (pressure drop) for this data set is that presented in this work. This specialized correlation is accurate to within 8% on average.

Acknowledgements

The authors appreciate the financial support for the data acquisition portion of this project provided by the Petroleum Research Fund and the National Science Foundation under Award No. CTS-0134510. Any opinions, findings, and conclusions or recommendations expressed in this material are those of the authors and do not necessarily reflect the views of the National Science Foundation.

References

[1] M.B. Ould Didi, N. Kattan, J.R. Thome, Prediction of two-phase pressure gradients of refrigerants inside horizontal tubes, Int. J. Refrig. 25 (2002) 935–947.
[2] R.C. Martinelli, D.B. Nelson, Prediction of pressure drop during forced circulation boiling of water, Trans. ASME 70 (1948) 695–702.
[3] R.W. Lockhart, R.C. Martinelli, Proposed correlation of data for isothermal two-phase, two-component flow in pipes, Chem. Eng. Prog. 45 (1) (1949) 39–48.
[4] G.B. Wallis, One-dimensional Two-phase Flow, McGraw-Hill, Inc., New York, 1969.
[5] J.C. Asali, G.W. Leman, T.J. Hanratty, Entrainment measurements and their use in design equations, PCH 6 (1/2) (1985) 207–221.
[6] E.T. Hurlburt, T.A. Newell, Prediction of the circumferential film thickness distribution in horizontal annular gas–liquid flow, J. Fluids Eng. 122 (2000) 1–7.
[7] D.G. Owen, G.F. Hewitt, An improved annular two-phase flow model, in: Third International Conference on Multi-Phase Flow, The Hague, Netherlands, May 1987, pp. 73–84.
[8] E.T. Hurlburt, L.B. Fore, R.C. Bauer, A two zone interfacial shear stress and liquid film velocity model for vertical annular two-phase flow, in: Proceedings of the ASME Fluids Engineering Division Summer Meeting 2006, Miami, FL, USA, vol. 2, 2006, pp. 677–684.
[9] H. Müller-Steinhagen, K. Heck, A simple friction pressure drop correlation for two-phase flow in pipes, Chem. Eng. Process. 20 (1986) 297–308.
[10] A.E. Dukler, M. Wicks III, R. Cleveland, Frictional pressure drop in two-phase flow: a comparison of existing correlations for pressure loss and holdup, AIChE J. 10 (1964) 38–43.
[11] F. Fu, J.F. Klausner, A separated flow model for predicting two-phase pressure drop and evaporative heat transfer for vertical annular flow, Int. J. Heat Fluid Flow 18 (1997) 541–549.
[12] W.H. Henstock, T.J. Hanratty, The interfacial drag and the height of the wall layer in annular flows, AIChE J. 22 (6) (1976) 990–1000.
[13] M.E.G. Ferguson, P.L. Spedding, Measurement and prediction of pressure drop in two-phase flow, J. Chem. Technol. Biotechnol. 62 (1995) 262–278.
[14] Z. Olujic, Predicting two-phase-flow friction loss in horizontal pipes, Chem. Eng. 92 (13) (1985) 45–50.
[15] W. Qu, I. Mudawar, Measurement and prediction of pressure drop in two-phase micro-channel heat sinks, Int. J. Heat Mass Transf. 46 (15) (2003) 2737–2753.
[16] I. Chen, R. Downing, E.G. Keshock, M. Al-Sharif, Measurements and correlation of two-phase pressure drop under microgravity conditions, J. Thermophys. Heat Transf. 5 (1991) 514–523.
[17] N.A. Vlachos, S.V. Paras, A.J. Karabelas, Liquid-to-wall shear stress distribution in stratified/atomization flow, Int. J. Multiphase Flow 23 (5) (1997) 845–863.
[18] A.H. Govan, G.F. Hewitt, D.G. Owen, G. Burnett, Wall shear stress measurements in vertical air–water annular two-phase flow, Int. J. Multiphase Flow 15 (3) (1989) 307–325.
[19] O. Okada, H. Fujita, Experimental studies of annular-mist flow in the nonequilibrium region of a long horizontal pipe (comparison between the mixing methods by a nozzle and a porous wall), FED – Adv. Gas–Liquid Flows 99 (1990) 57–64.
[20] T.A. Shedd, T.A. Newell, Automated optical liquid film thickness measurement method, Rev. Sci. Instrum. 69 (12) (1998) 4205–4213.
[21] D.J. Rodíguez, T.A. Shedd, Cross-sectional imaging of the liquid film in horizontal two-phase annular flow, in: 2004 ASME Heat Transfer/Fluids Engineering Summer Conference, Charlotte, NC, July 2004, Paper 56445.
[22] N.J. Hawkes, C.J. Lawrence, G.F. Hewitt, Studies of wispy-annular flow using transient pressure gradient and optical measurements, Int. J. Multiphase Flow 26 (2000) 1565–1582.
[23] L.B. Fore, S.G. Beus, R.C. Bauer, Interfacial friction in gas–liquid annular flow: analogies to full transition and roughness, Int. J. Multiphase Flow 26 (2000) 1755–1769.
[24] I. Kataoka, M. Ishiii, A. Nakayama, Entrainment and deposition rates of droplets in annular two-phase flow, Int. J. Heat Mass Transf. 43 (2000) 1573–1589.
[25] R.W. Swanson, Characteristics of the Gas–Liquid Interface in Two-phase Annular Flow, Ph.D. Thesis, University of Delaware, Delaware, June 1966.
[26] T. Sawai, S. Yamauchi, S. Nakanishi, Behavior of disturbance waves under hydrodynamic non-equilibrium conditions, Int. J. Multiphase Flow 15 (3) (1989) 341–356.
[27] B.J. Azzopardi, Disturbance wave frequencies, velocities and spacing in vertical annular two-phase flow, Nucl. Eng. Des. 92 (2) (1986) 121–133.
[28] B.J. Azzopardi, Drops in annular two-phase flow, Int. J. Multiphase Flow 23 (Supplement) (1997) 1–53.
[29] D. Schubring, T.A. Shedd, Wave behavior in horizontal annular flow, Int. J. Multiphase Flow 34 (7) (2008) 636–646.
[30] J.E. Laurinat, Studies on the Effects of Pipe Size on Horizontal Annular Two-Phase Flows. Ph.D. thesis, University of Illinois at Urbana-Champaign, Urbana, IL, July 1982.